Theory and applications of magnetic field line helicity in Solar Physics

Kostas Moraitis
University of Ioannina, Greece

5th Hel.A.S. Summer School
"Magnetohydrodynamics in Astrophysics"
Ioannina, 16-20 September 2024

Πανεπιστήμιο
Ιωαννίνων

Outline

- Introduction
  - Magnetic helicity – Relative magnetic helicity
  - Definition and properties of field line helicity – relative field line helicity
  - Computation of RFLH
- Applications of field line helicity
  - In idealized solar situations
  - In the global magnetic field
  - In solar active regions
  - RFLH as an indicator of solar eruptivity
- Summary

Outline

- **Introduction**
  - Magnetic helicity – Relative magnetic helicity
  - Definition and properties of field line helicity – relative field line helicity
  - Computation of RFLH
- Applications of field line helicity
  - In idealized solar situations
  - In the global magnetic field
  - In solar active regions
  - RFLH as an indicator of solar eruptivity
- Summary

Magnetic helicity

- Magnetic helicity is a geometrical measure of the twist and writhe of the magnetic field lines, and of the intertwining between pairs of lines (Gauss linking number)
- Mathematically, it is defined through the vector potential **A**, as

$$H_\mathrm{m} = \int_V \mathbf{A} \cdot \mathbf{B} \, \mathrm{d}V$$

- Signed scalar quantity (right (+), or left (-) handed) with units of magnetic flux squared (Wb^2/Mx^2 in SI/cgs)
- Conserved in ideal MHD (Woltjer 1958); slower-than-energy deteriorating in resistive MHD (Taylor 1975; Pariat et al. 2015)
- Topological invariant; links cannot change by ‘frozen’ magnetic field lines
- Coronal mass ejections are caused by the need to expel the excess helicity accumulated in the corona (Rust 1994)

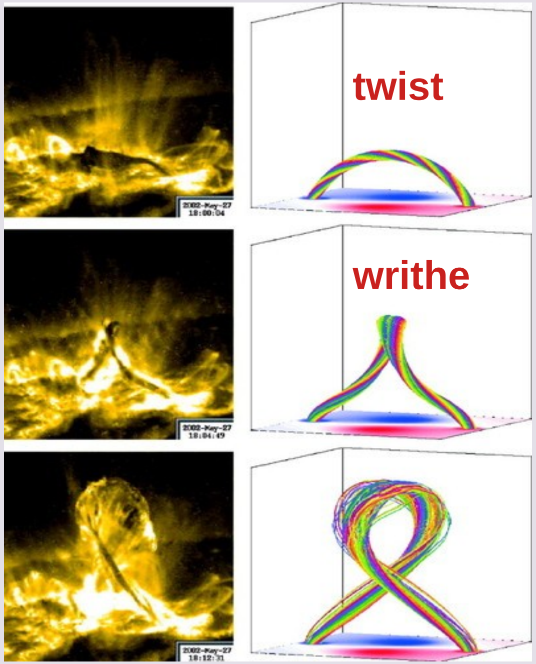

Török & Kliem 2005

Wiegelmann & Sakurai 2012

Relative magnetic helicity

Magnetic helicity is well defined (gauge independent) for closed ***B***

$$H_\mathrm{m} = \int_V \mathbf{A}\cdot\mathbf{B}\,\mathrm{d}V \xrightarrow{\mathbf{A}'=\mathbf{A}+\nabla\xi} H'_\mathrm{m} = H_\mathrm{m} + \oint_{\partial V} \xi\mathbf{B}\cdot\mathrm{d}\mathbf{S}$$

$$H'_\mathrm{m} = H_\mathrm{m} \Rightarrow \hat{n}\cdot\mathbf{B}|_{\partial V} = 0$$

In astrophysical conditions, the appropriate form is relative magnetic helicity

$$H_\mathrm{r} = \int_V (\mathbf{A}+\mathbf{A}_\mathrm{p})\cdot(\mathbf{B}-\mathbf{B}_\mathrm{p})\,\mathrm{d}V$$

which is gauge independent for closed $\boldsymbol{B}$-$\boldsymbol{B}_\mathbf{p}$

$$\hat{n}\cdot\mathbf{B}|_{\partial V} = \hat{n}\cdot\mathbf{B}_\mathrm{p}|_{\partial V}$$

Usually, reference field=potential (no current → no helicity)
RMH is a single number that characterizes the whole volume

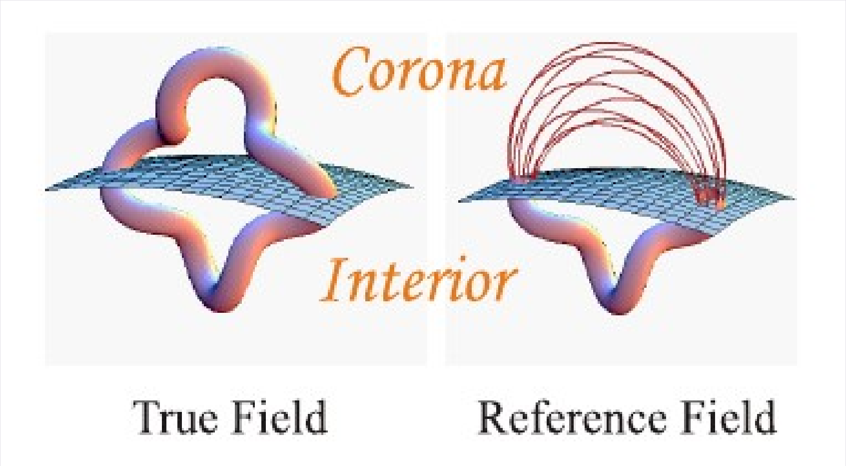

Berger & Field 1984; Finn & Antonsen 1985;

Field line helicity

- Magnetic helicity provides no spatial information about the locations where helicity is more important
- A density for magnetic helicity cannot be defined since the vector potential is a non-local quantity
- A good proxy for the density of magnetic helicity is field line helicity (FLH), that can be defined as the *magnetic helicity per unit of magnetic flux* of a single field line

$$
\begin{aligned}
h(C) &= \lim_{\epsilon \to 0} \left(\frac{1}{\Phi_\epsilon} \int_{V_\epsilon} \mathbf{A} \cdot \mathbf{B} \, \mathrm{d}V \right) \\
&= \lim_{\epsilon \to 0} \left(\frac{1}{\Phi_\epsilon} \int_{V_\epsilon} (\mathbf{A} \cdot \mathrm{d}\boldsymbol{l}) \, \mathrm{d}\Phi \right) \\
&= \int_C \mathbf{A} \cdot \mathrm{d}\boldsymbol{l}
\end{aligned}
$$

$$
\begin{aligned}
&(\mathbf{A} \cdot \mathbf{B}) \, \mathrm{d}V = \\
&(\mathbf{A} \cdot \mathbf{B}) \, (\mathrm{d}\mathbf{S} \cdot \mathrm{d}\boldsymbol{l}) = \\
&(\mathbf{A} \cdot \mathrm{d}\boldsymbol{l}) \, (\mathbf{B} \cdot \mathrm{d}\mathbf{S}) = \\
&(\mathbf{A} \cdot \mathrm{d}\boldsymbol{l}) \, \mathrm{d}\Phi
\end{aligned}
$$

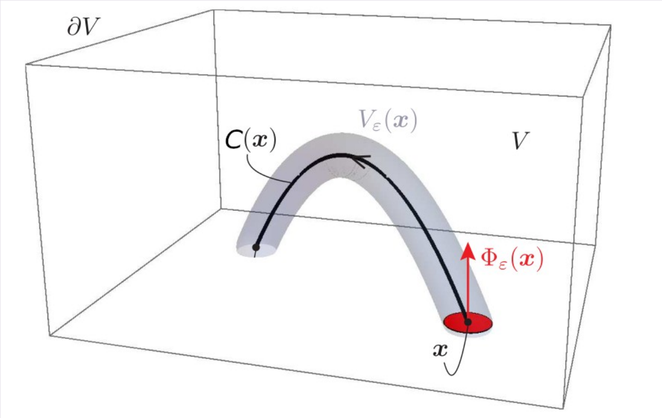

Yeates & Page 2018

FLH properties

- FLH has units of magnetic flux (Wb/Mx in SI/cgs)
- FLH is:
  - unique for each field line
  - gauge-dependent for open field lines
  - the magnetic flux through the surface bounded by the field line, for closed field lines

$$h(C;\mathbf{A}) = \begin{cases} \int_{c_+}^{c_-} \mathbf{A}\cdot \mathrm{d}\boldsymbol{l}, & C \text{ open} \\ \oint_C \mathbf{A}\cdot \mathrm{d}\boldsymbol{l} = \Phi, & C \text{ closed} \end{cases}$$

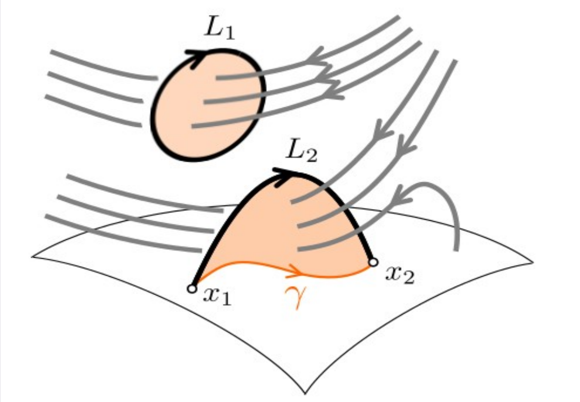

Yeates & Hornig 2016

- With the help of FLH magnetic helicity reduces to a surface integral along the boundary

$$H_\mathrm{m} = \oint_{\partial V} h\,\mathrm{d}\Phi$$

- It can also be considered as the:
  - flux per field line (Antiochos 1987)
  - average angle through which other field lines wrap around the given field line (Berger 1988)
  - topological flux function, action of the Hamiltonian system of the field lines (Yeates & Hornig, 2013; 2014)

Derivation of relative FLH

$$
\begin{aligned}
H_\mathrm{r} &= \int_V (\mathbf{A}+\mathbf{A}_\mathrm{p})\cdot(\mathbf{B}-\mathbf{B}_\mathrm{p})\,\mathrm{d}V \\
&= \int_V (\mathbf{A}+\mathbf{A}_\mathrm{p})\cdot\mathbf{B}\,\mathrm{d}V - \int_V (\mathbf{A}+\mathbf{A}_\mathrm{p})\cdot\mathbf{B}_\mathrm{p}\,\mathrm{d}V \\
&= \oint_{\partial V^+}\left(\int_{\alpha_+}^{\alpha_-}(\mathbf{A}+\mathbf{A}_\mathrm{p})\cdot\mathrm{d}\boldsymbol{l}\right)\mathrm{d}\Phi - \oint_{\partial V^+}\left(\int_{\alpha_{p+}}^{\alpha_{p-}}(\mathbf{A}+\mathbf{A}_\mathrm{p})\cdot\mathrm{d}\boldsymbol{l}_\mathrm{p}\right)\mathrm{d}\Phi_\mathrm{p} \\
&= \oint_{\partial V^+}\left(\int_{\alpha_+}^{\alpha_-}(\mathbf{A}+\mathbf{A}_\mathrm{p})\cdot\mathrm{d}\boldsymbol{l} - \int_{\alpha_+}^{\alpha_{p-}}(\mathbf{A}+\mathbf{A}_\mathrm{p})\cdot\mathrm{d}\boldsymbol{l}_\mathrm{p}\right)\mathrm{d}\Phi \\
&= \oint_{\partial V^+} h_\mathrm{r}^+\,\mathrm{d}\Phi
\end{aligned}
$$

flux-tube assumption

$$
\begin{aligned}
&(\mathbf{A}\cdot\mathbf{B})\,\mathrm{d}V = \\
&(\mathbf{A}\cdot\mathbf{B})\,(\mathrm{d}\mathbf{S}\cdot\mathrm{d}\boldsymbol{l}) = \\
&(\mathbf{A}\cdot\mathrm{d}\boldsymbol{l})\,(\mathbf{B}\cdot\mathrm{d}\mathbf{S}) = \\
&(\mathbf{A}\cdot\mathrm{d}\boldsymbol{l})\,\mathrm{d}\Phi
\end{aligned}
$$

$$\partial V^\pm = \{\mathbf{x}\in\partial V : \hat{n}\cdot\mathbf{B}(\mathbf{x}) \lessgtr 0\}$$

start from same footpoint $\alpha_{p+}=\alpha_+$

so that $\mathrm{d}\Phi = \mathrm{d}\Phi_\mathrm{p}$ since

$$|\hat{n}\cdot\mathbf{B}| = |\hat{n}\cdot\mathbf{B}_\mathrm{p}|$$

- Field lines that close within the volume do not enter in this calculation

Relative field line helicity

We can similarly define two other RFLHs depending on the part of the boundary considered:

$$H_r = \oint_{\partial V^+} h_r^+ \, d\Phi = \oint_{\partial V^-} h_r^- \, d\Phi = \oint_{\partial V} h_r \, d\Phi$$

whole boundary $h_r = \frac{1}{2}\left(h_r^+ + h_r^-\right)$

(+) polarity $h_r^+ = \int_{\alpha_+}^{\alpha_-} (\mathbf{A} + \mathbf{A}_p) \cdot d\boldsymbol{l} - \int_{\alpha_+}^{\alpha_{p-}} (\mathbf{A} + \mathbf{A}_p) \cdot d\boldsymbol{l}_p$

(-) polarity $h_r^- = \int_{\alpha_+}^{\alpha_-} (\mathbf{A} + \mathbf{A}_p) \cdot d\boldsymbol{l} - \int_{\alpha_{p+}}^{\alpha_-} (\mathbf{A} + \mathbf{A}_p) \cdot d\boldsymbol{l}_p$

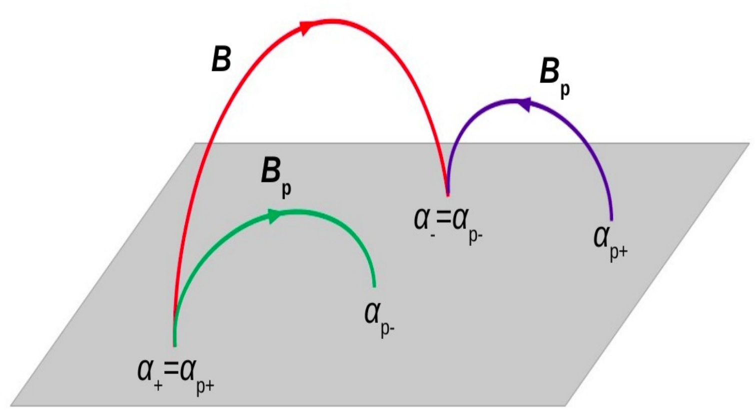

In all cases, RFLH involves two set of field lines, of **B** and of $\mathbf{B}_p$,
and recovers relative helicity when summed over the respective boundary

RFLH components

$$H_\mathrm{r} = \int_V (\mathbf{A} + \mathbf{A}_\mathrm{p}) \cdot (\mathbf{B} - \mathbf{B}_\mathrm{p})\, \mathrm{d}V$$

$$H_\mathrm{r} = H_\mathrm{j} + H_\mathrm{pj}$$

$$H_\mathrm{j} = \int_V (\mathbf{A} - \mathbf{A}_\mathrm{p}) \cdot (\mathbf{B} - \mathbf{B}_\mathrm{p})\, \mathrm{d}V$$

current-carrying component
(self helicity)

$$H_\mathrm{pj} = 2\int_V \mathbf{A}_\mathrm{p} \cdot (\mathbf{B} - \mathbf{B}_\mathrm{p})\, \mathrm{d}V$$

volume-threading component
(mutual helicity)

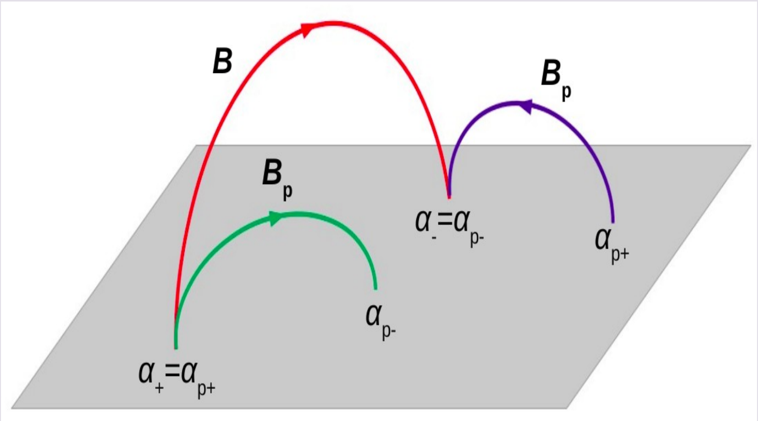

Berger 1999; Linan et al. 2018

$$H_\mathrm{j} = \oint_{\partial V+} h_\mathrm{j}^+\, \mathrm{d}\Phi = \oint_{\partial V-} h_\mathrm{j}^-\, \mathrm{d}\Phi = \oint_{\partial V} h_\mathrm{j}\, \mathrm{d}\Phi$$

$$h_\mathrm{j}^+ = \int_{\alpha_+}^{\alpha_-} (\mathbf{A} - \mathbf{A}_\mathrm{p}) \cdot \mathrm{d}\boldsymbol{l} - \int_{\alpha_+}^{\alpha_{p-}} (\mathbf{A} - \mathbf{A}_\mathrm{p}) \cdot \mathrm{d}\boldsymbol{l}_\mathrm{p}$$

current-carrying FLH

$$H_\mathrm{pj} = \oint_{\partial V+} h_\mathrm{pj}^+\, \mathrm{d}\Phi = \oint_{\partial V-} h_\mathrm{pj}^-\, \mathrm{d}\Phi = \oint_{\partial V} h_\mathrm{pj}\, \mathrm{d}\Phi$$

$$h_\mathrm{pj}^+ = 2\int_{\alpha_+}^{\alpha_-} \mathbf{A}_\mathrm{p} \cdot \mathrm{d}\boldsymbol{l} - 2\int_{\alpha_+}^{\alpha_{p-}} \mathbf{A}_\mathrm{p} \cdot \mathrm{d}\boldsymbol{l}_\mathrm{p}$$

volume-threading FLH

Computation of RFLH

$$h_\mathrm{r}^+ = \int_{\alpha_+}^{\alpha_-} (\mathbf{A} + \mathbf{A}_\mathrm{p}) \cdot \mathrm{d}\boldsymbol{l} - \int_{\alpha_+}^{\alpha_{p-}} (\mathbf{A} + \mathbf{A}_\mathrm{p}) \cdot \mathrm{d}\boldsymbol{l}_\mathrm{p}$$

$$H_\mathrm{r} = \oint_{\partial V^+} h_\mathrm{r}^+ \, \mathrm{d}\Phi$$

$$H_\mathrm{r} = \int_V (\mathbf{A} + \mathbf{A}_\mathrm{p}) \cdot (\mathbf{B} - \mathbf{B}_\mathrm{p}) \, \mathrm{d}V$$

Instantaneous, finite-volume method

Input : ***B***, grid

Requires: 2x fl integrations + ***A***, $\boldsymbol{A}_\mathbf{p}$ ← ***B***, $\boldsymbol{B}_\mathbf{p}$

Steps:

1. ***B*** → $\boldsymbol{B}_\mathbf{p}$
2. ***B***, $\boldsymbol{B}_\mathbf{p}$ → ***A***, $\boldsymbol{A}_\mathbf{p}$
3. fl integrations along ***B***, $\boldsymbol{B}_\mathbf{p}$

Computation of RFLH

$$h_{\mathrm{r}}^{+} = \int_{\alpha_+}^{\alpha_-} (\mathbf{A} + \mathbf{A}_{\mathrm{p}}) \cdot \mathrm{d}\boldsymbol{l} - \int_{\alpha_+}^{\alpha_{p-}} (\mathbf{A} + \mathbf{A}_{\mathrm{p}}) \cdot \mathrm{d}\boldsymbol{l}_{\mathrm{p}}$$

$$H_{\mathrm{r}} = \oint_{\partial V^+} h_{\mathrm{r}}^{+}\, \mathrm{d}\Phi$$

$$H_{\mathrm{r}} = \int_V (\mathbf{A} + \mathbf{A}_{\mathrm{p}}) \cdot (\mathbf{B} - \mathbf{B}_{\mathrm{p}})\, \mathrm{d}V$$

Instantaneous, finite-volume method

Input : ***B***, grid

Requires: 2x fl integrations + ***A***, $\boldsymbol{A}_{\mathbf{p}}$ ← ***B***, $\boldsymbol{B}_{\mathbf{p}}$

Steps:

1. ***B*** → $\boldsymbol{B}_{\mathbf{p}}$
2. ***B***, $\boldsymbol{B}_{\mathbf{p}}$ → ***A***, $\boldsymbol{A}_{\mathbf{p}}$
3. fl integrations along ***B***, $\boldsymbol{B}_{\mathbf{p}}$

Compute potential magnetic field under gauge invariance condition

$$\mathbf{B}_{\mathrm{p}} = \nabla\Phi$$
$$\hat{n} \cdot \mathbf{B}_{\mathrm{p}}|_{\partial V} = \hat{n} \cdot \mathbf{B}|_{\partial V}$$

→

$$\nabla^2\Phi = 0$$
$$\left.\frac{\partial\Phi}{\partial\hat{n}}\right|_{\partial V} = \hat{n} \cdot \mathbf{B}|_{\partial V}$$

solution of Laplace's equation under Neumann BCs

- Trivial problem in Cartesian coordinates, different numerical libraries using FFT method in non-homogeneous, uniform grid
- It can also be done in spherical and cylindrical
- For non-uniform grid, interpolation to and from a uniform grid is required

Computation of RFLH

$$h_\mathrm{r}^+ = \int_{\alpha_+}^{\alpha_-} (\mathbf{A}+\mathbf{A}_\mathrm{p})\cdot \mathrm{d}\boldsymbol{l} - \int_{\alpha_+}^{\alpha_{p-}} (\mathbf{A}+\mathbf{A}_\mathrm{p})\cdot \mathrm{d}\boldsymbol{l}_\mathrm{p}$$

$$H_\mathrm{r} = \oint_{\partial V+} h_\mathrm{r}^+ \,\mathrm{d}\Phi$$

$$H_\mathrm{r} = \int_V (\mathbf{A}+\mathbf{A}_\mathrm{p})\cdot(\mathbf{B}-\mathbf{B}_\mathrm{p})\,\mathrm{d}V$$

Instantaneous, finite-volume method

Input : ***B***, grid

Requires: 2x fl integrations + $\boldsymbol{A}$, $\boldsymbol{A}_\mathbf{p}$ ← $\boldsymbol{B}$, $\boldsymbol{B}_\mathbf{p}$

Steps:

1. $\boldsymbol{B} \rightarrow \boldsymbol{B}_\mathbf{p}$
2. $\boldsymbol{B}$, $\boldsymbol{B}_\mathbf{p} \rightarrow \boldsymbol{A}$, $\boldsymbol{A}_\mathbf{p}$
3. fl integrations along $\boldsymbol{B}$, $\boldsymbol{B}_\mathbf{p}$

Computation of vector potentials by inversion of $\mathbf{B} = \nabla\times\mathbf{A}$ with Valori et al. 2012 method which uses DeVore (2000) gauge $\hat{\mathbf{z}}\cdot\mathbf{A} = 0$

$$\mathbf{A}(x,y,z) = \boldsymbol{\alpha}(x,y) + \hat{\mathbf{z}}\times\int_{z_0}^{z} \mathrm{d}z'\,\mathbf{B}(x,y,z')$$

$$\nabla_\perp\times\boldsymbol{\alpha} = B_z(x,y,z_0)$$

DV simple gauge (DVS)

$$\alpha_y(x,y) = c\int_{x_0}^{x}\mathrm{d}x'\,B_z(x',y,z_0)$$

$$\alpha_x(x,y) = -(1-c)\int_{y_0}^{y}\mathrm{d}y'\,B_z(x,y',z_0)$$

$$c\in[0,1]$$

DV Coulomb gauge (DVC)

$$\nabla_\perp\cdot\boldsymbol{\alpha} = 0 \qquad \boldsymbol{\alpha} = \hat{\mathbf{z}}\times\nabla_\perp u$$

$$\nabla_\perp^2 u = B_z(x,y,z_0)$$

- Same method for both vector potentials
- Reference plane $z=z_0$ important
- Integrations: trapezoidal rule, applicable also to non-uniform grid
- 2D Poisson problem similarly to 3D Laplace

Computation of RFLH

$$h_r^+ = \int_{\alpha_+}^{\alpha_-} (\mathbf{A} + \mathbf{A}_p) \cdot \mathrm{d}\boldsymbol{l} - \int_{\alpha_+}^{\alpha_{p-}} (\mathbf{A} + \mathbf{A}_p) \cdot \mathrm{d}\boldsymbol{l}_p$$

$$H_r = \oint_{\partial V^+} h_r^+ \, \mathrm{d}\Phi$$

$$H_r = \int_V (\mathbf{A} + \mathbf{A}_p) \cdot (\mathbf{B} - \mathbf{B}_p) \, \mathrm{d}V$$

Instantaneous, finite-volume method

Input : ***B***, grid

Requires: 2x fl integrations + ***A***, $\boldsymbol{A}_\mathbf{p}$ ← ***B***, $\boldsymbol{B}_\mathbf{p}$

Steps:

1. ***B*** → $\boldsymbol{B}_\mathbf{p}$
2. ***B***, $\boldsymbol{B}_\mathbf{p}$ → ***A***, $\boldsymbol{A}_\mathbf{p}$
3. fl integrations along ***B***, $\boldsymbol{B}_\mathbf{p}$

- Variety of fl integration routines
- Modification of QSL Squasher code (Tassev & Savcheva 2016) which uses adaptive RK in C++, fast and robust
- Augment system of equations with

$$\frac{\mathrm{d}h}{\mathrm{d}s} = \frac{(\mathbf{A} + \mathbf{A}_p) \cdot \mathbf{B}}{B}$$

- Same method for both field line integrations
- Consider only photosphere
- RFLH more computationally-demanding than relative helicity
- RFLH components can be computed the same way

Importance of gauge choice

- RFLH is gauge-dependent for open field lines
- The choice of gauge:
  - determines how to close field lines on the boundary
  - changes equations
  - imposes physical meaning
  - simplifies computations

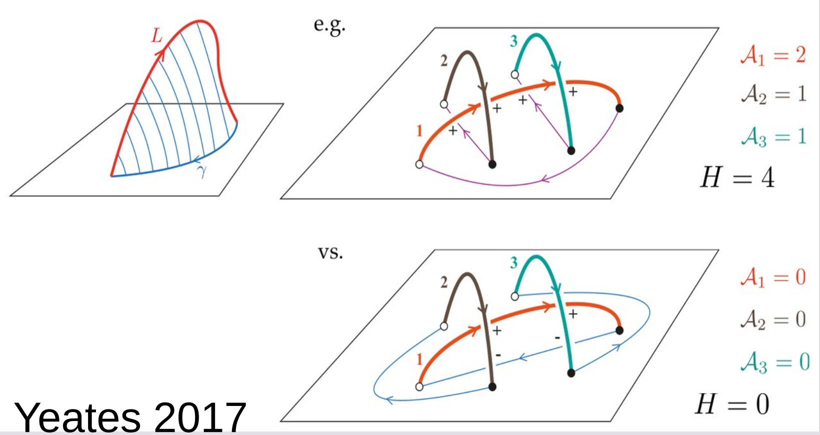

Yeates 2017

$$H_{\rm r} = \int_V (\mathbf{A} + \mathbf{A}_{\rm p}) \cdot (\mathbf{B} - \mathbf{B}_{\rm p})\, {\rm d}V$$

$$h_{\rm r}^{+} = \int_{\alpha_+}^{\alpha_-} (\mathbf{A} + \mathbf{A}_{\rm p}) \cdot {\rm d}\boldsymbol{l} - \int_{\alpha_+}^{\alpha_{p-}} (\mathbf{A} + \mathbf{A}_{\rm p}) \cdot {\rm d}\boldsymbol{l}_{\rm p}$$

DV gauge (Moraitis et al. 2019)
A in DVS, $\boldsymbol{A}_{\mathbf{p}}$ in DVC

$$H_{\rm r} = \int_V \mathbf{A} \cdot \mathbf{B}\, {\rm d}V - \int_V \mathbf{A}_{\rm p} \cdot \mathbf{B}_{\rm p}\, {\rm d}V + \int_V (\mathbf{A}_{\rm p} \cdot \mathbf{B} - \mathbf{A} \cdot \mathbf{B}_{\rm p})\, {\rm d}V$$

$$H_{\rm r} = \int_V \mathbf{A} \cdot \mathbf{B}\, {\rm d}V - \int_V \mathbf{A}_{\rm p} \cdot \mathbf{B}_{\rm p}\, {\rm d}V + \oint_{\partial V} (\mathbf{A} \times \mathbf{A}_{\rm p}) \cdot {\rm d}\mathbf{S}$$

$$\hat{n} \times \mathbf{A}_{\rm p}|_{\partial V} = \hat{n} \times \mathbf{A}|_{\partial V}$$

$$h_{\rm r}^{\rm BF,+} = \int_{\alpha_+}^{\alpha_-} \mathbf{A} \cdot {\rm d}\boldsymbol{l} - \int_{\alpha_+}^{\alpha_{p-}} \mathbf{A}_{\rm p} \cdot {\rm d}\boldsymbol{l}_{\rm p}$$

BF gauge (Yeates & Page 2018)

Outline

- Introduction
  - Magnetic helicity – Relative magnetic helicity
  - Definition and properties of field line helicity – relative field line helicity
  - Computation of RFLH
- **Applications of field line helicity**
  - In idealized solar situations
  - In the global magnetic field
  - In solar active regions
  - RFLH as an indicator of solar eruptivity
- Summary

Idealized applications I

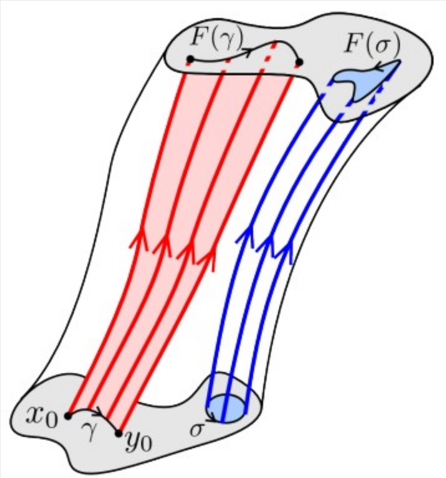

Yeates & Hornig 2013; 2014

Magnetic braids = non-zero, line-tied magnetic fields whose field lines all connect between two boundaries
Model of coronal loops
FLH:

$$\mathcal{A}(x_0) = \int_{x_0}^{F(x_0)} \mathbf{A}\big(f(x_0; z)\big) \cdot \,\mathrm{d}\mathbf{l}$$

- Measures the average poloidal magnetic flux around any given field line, or the average pairwise crossing number between a given field line and all others
- Ideal invariant under specific gauge

$$\mathbf{n} \times \mathbf{A}|_{\partial V} = \mathbf{n} \times \mathbf{A}^{\mathrm{ref}}|_{\partial V}$$

$$\frac{\mathrm{d}\mathcal{A}}{\mathrm{d}t} = \int_{x_0}^{F(x_0)} \nabla(\Phi + \mathbf{v} \cdot \mathbf{A}) \cdot \,\mathrm{d}\mathbf{l} = 0$$

- Gives relative helicity when integrated over ‘photosphere’
- Uniquely characterizes field line mapping and magnetic topology

$$H_r - H^{\mathrm{ref}} = \int_{D_0} \mathcal{A}(x_0) B_z(x_0) \,\mathrm{d}^2 x_0$$

Idealized applications II

Evolution of FLH during magnetic reconnection

$$
\begin{aligned}
\frac{\mathrm{d}\mathcal{A}(\vec{x},t)}{\mathrm{d}t} &= \frac{\mathrm{d}}{\mathrm{d}t}\int_{F(\vec{x},t)} \vec{A}\cdot\mathrm{d}\vec{l} \\
&= \int_{F(\vec{x},t)} \left[\frac{\partial\vec{A}}{\partial t} - \vec{w}\times\nabla\times\vec{A} + \nabla\left(\vec{w}\cdot\vec{A}\right)\right]\cdot\mathrm{d}\vec{l} \\
&= \int_{F(\vec{x},t)} \nabla\left(\vec{w}\cdot\vec{A} - \Psi - \Phi\right)\cdot\mathrm{d}\vec{l} \\
&= \left[\vec{w}\cdot\vec{A} - \Psi - \Phi\right]_{\vec{x}_0}^{\vec{x}_1}
\end{aligned}
$$

Russel et al. 2015

motion of fl on boundaries:
in both ideal and reconnection,
gauge-dependent
voltage drop along fl
electric potential: can be eliminated
by gauge choice

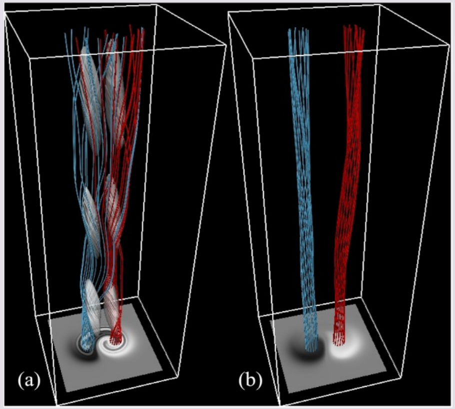

MHD simulation of magnetic braids' relaxation

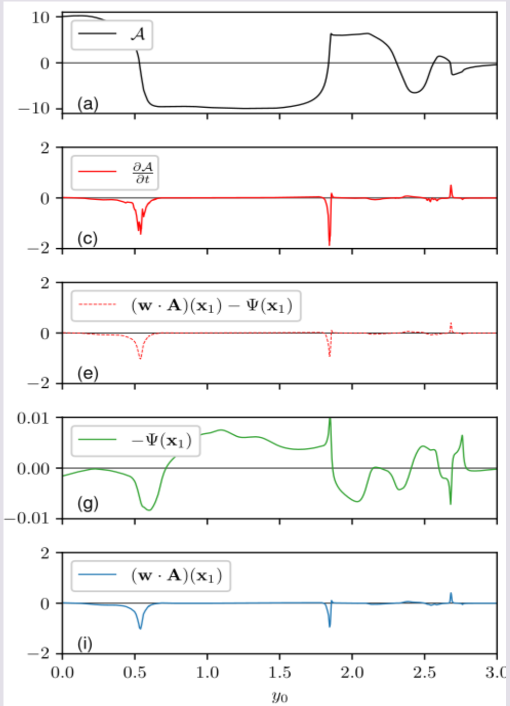

Yeates et al. 2021

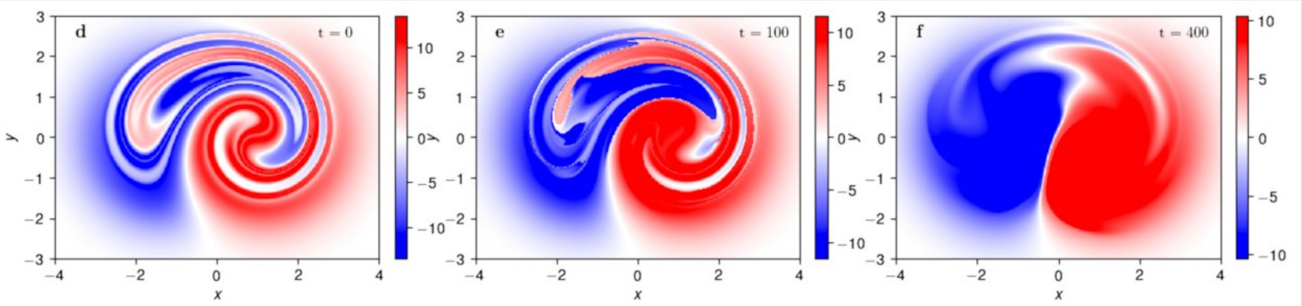

Mathematical applications

Theorem 1. *Let* $\mathbf{v}, \mathbf{v}'$ *be two braided vector fields on the same domain* $\mathcal{M}$ *whose field lines on* S_s *are linked by an end-vanishing isotopy. Then the field lines of* $\mathbf{v}$ *and those of* $\mathbf{v}'$ *within* $\mathcal{M}$ *can be linked by an end-vanishing isotopy if and only if* $L_{\mathbf{v}} = L_{\mathbf{v}'}$ *on all of* D_0.

Prior & Yeates 2021
topological characterisation of braided vector fields through field line winding

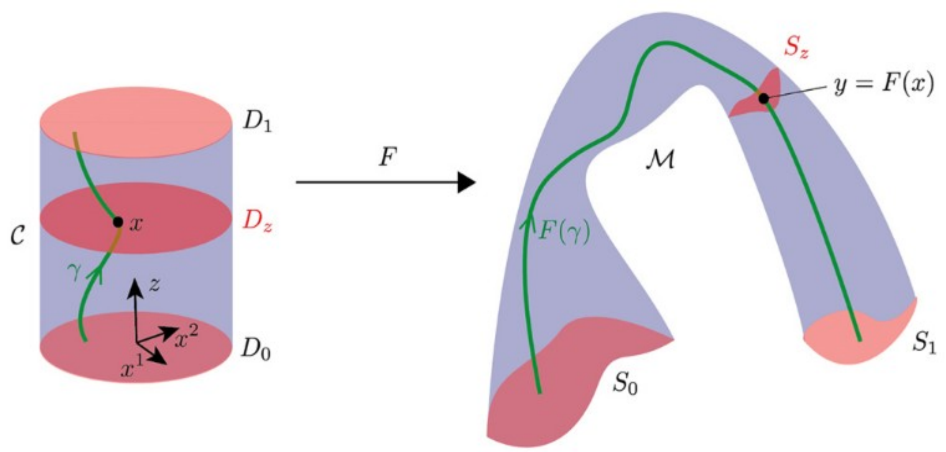

tubular subdomain = embedding of the unit cylinder

$$H = \int_{\mathcal{S}^+} \varepsilon^{kj} \partial_k X^i \widetilde{C_{ri}} C_{rj} \mathrm{d}x^1 \mathrm{d}x^2 - H_r$$

Aly 2018
tangential components of $\boldsymbol{C}_r$
magnetic mapping

The global magnetic field of the Sun

Time-dependent, nonpotential simulation of global coronal ***B***
magnetofrictional method
photospheric driving (differential rotation + supergranular diffusion, no flux emergence)
Initially, ***B***=$\boldsymbol{B}_{\mathbf{p}}$ from realistic distribution of magnetic flux

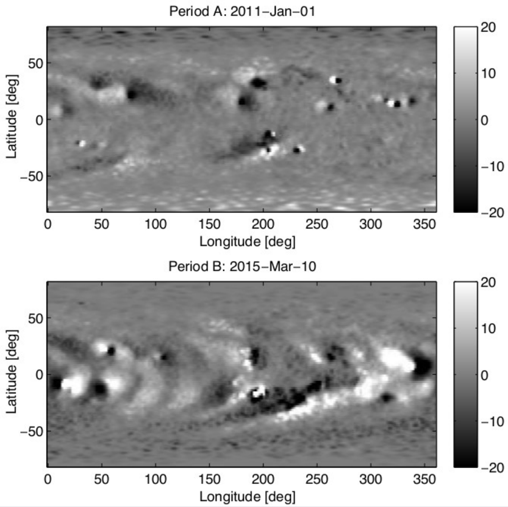

Yeates & Hornig 2016

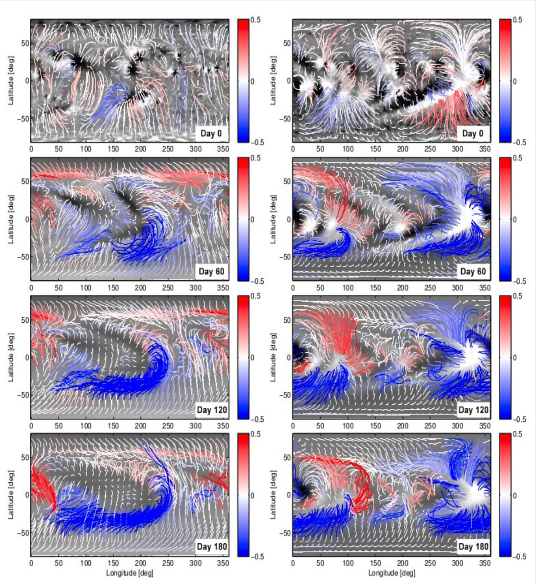

continuous sequence of near force-free equilibria
build up of large-scale electric currents, concentrated in magnetic flux ropes

non-uniform distribution of FLH:
In open fls, FLH is lost
In closed fls, FLH is stored in twisted flux ropes which eventually erupt

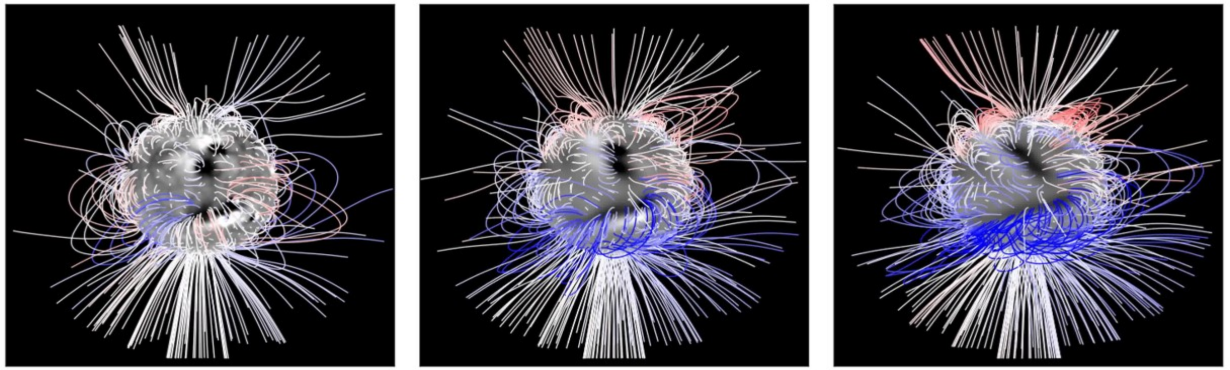

Flux rope identification

15-year simulation (1996-2012) of global ***B***
with the same magnetofrictional method,
but with the insertion of 2040 bipolar regions

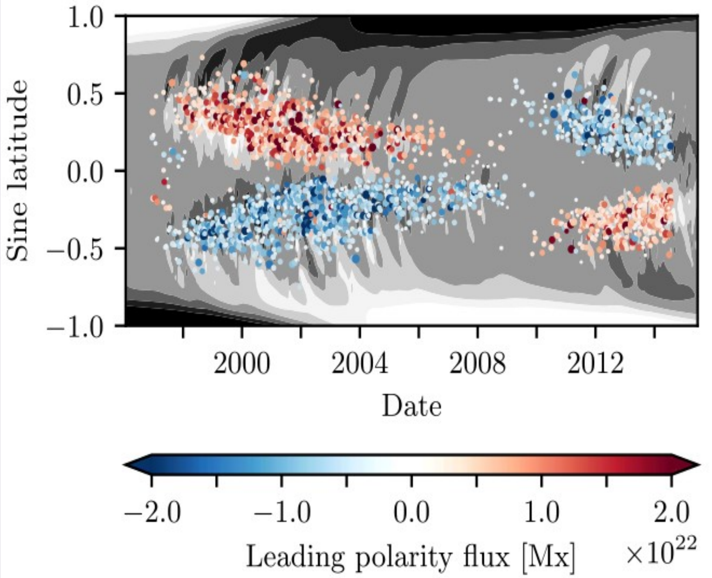

Lowder & Yeates 2017

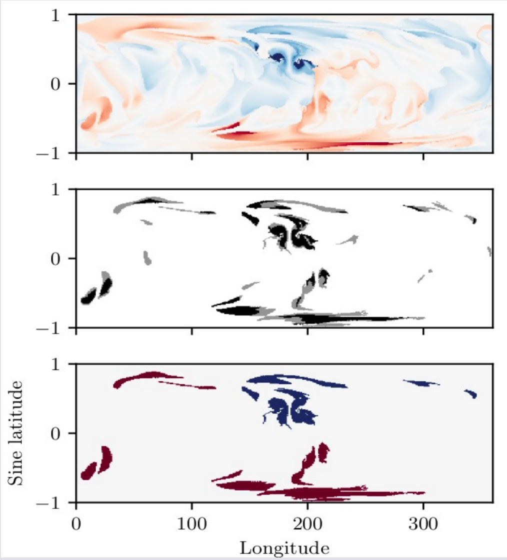

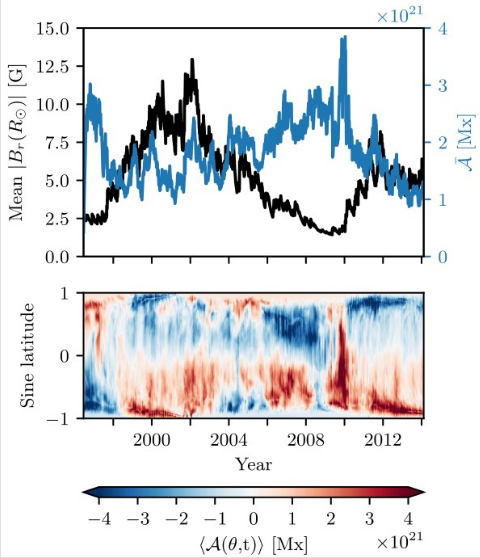

Flux rope identification through
mean unsigned FLH values
core+envelope thresholds
ref values simulation-specific
>1500 eruptive + >2000 non-eruptive
flux ropes detected

$$\tau_c(t) = \frac{\overline{\mathcal{A}}(t)}{\overline{\mathcal{A}}_{\text{ref}}}\tau_{c,\text{ref}}; \quad \tau_e(t) = \frac{\overline{\mathcal{A}}(t)}{\overline{\mathcal{A}}_{\text{ref}}}\tau_{e,\text{ref}}$$

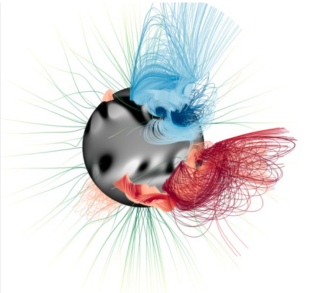

Solar active region 11158

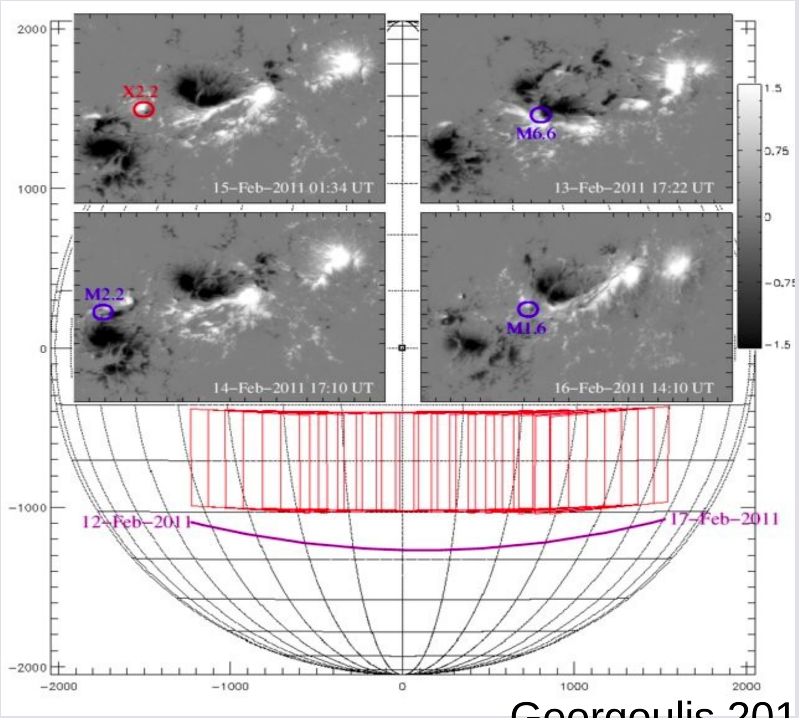

Georgoulis 2013

1st SDO/HMI AR
12-17 Feb 2011
3 M-class flares + an X2.2, all eruptive

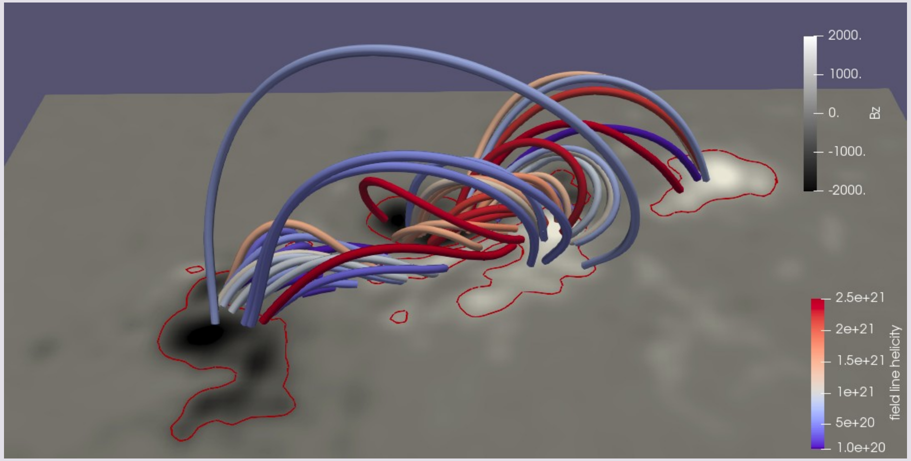

15 Feb 2011, 01:11 UT

<u>Coronal magnetic field modelling</u>
NLFF extrapolation (Thalmann et al. 2019)
215 Mm x 130 Mm x 185 Mm
resolution 2’’ per pixel, 12 min cadence
High-quality reconstruction (high solenoidality), essential for reliable helicity values (Valori et al. 2016)

RFLH during the X-flare of AR 11158

RFLH **RFLH differences**

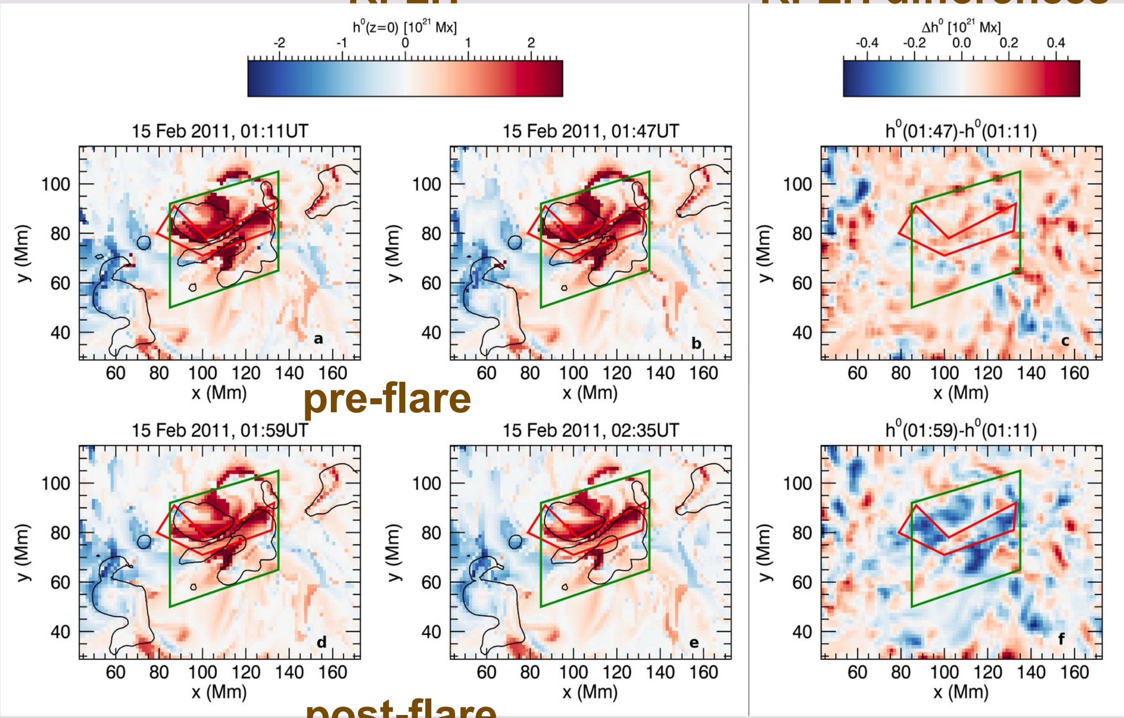

pre-flare

post-flare

Moraitis et al. 2021

- RFLH highlights important locations for eruptions (e.g., flare ribbons)
- RFLH can be used to compute the helicity of an arbitrarily-shaped ROI
- Green box contains almost the same helicity as whole FOV
- Red box contains half the helicity
- All curves drop by 20-25%

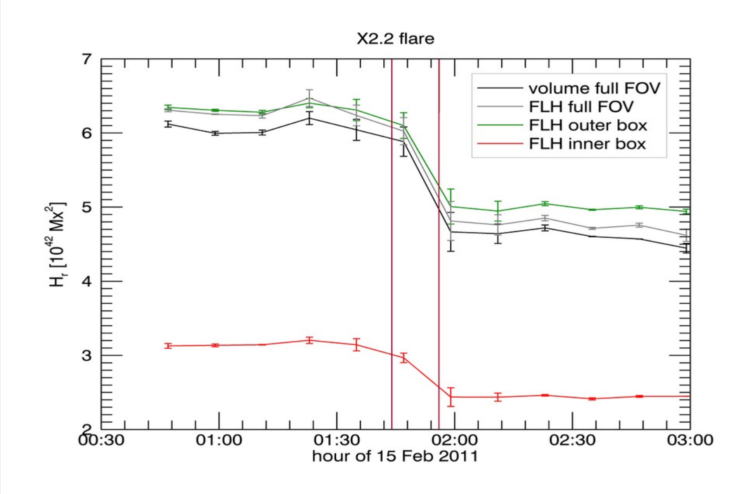

The AR sample

AR 11158, Feb 2011, 4 days, 115 snapshots, 1X+2M flares
AR 11261, Aug 2011, 12 hours, 60 snapshots, 1M flare
AR 11429, Mar 2012, 2 days, 47 snapshots, 2X+7M flares
AR 11520, Jul 2012, 12 hours, 61 snapshots, 1X flare
AR 11618, Nov 2012, 6.5 days, 675 snapshots, 4M flares
AR 11890, Nov 2013, 7.5 days, 892 snapshots, 3X+4M flares
AR 12014, Mar 2014, 12 hours, 60 snapshots, C flares
AR 12192, Oct 2014, 4.5 days, 198 snapshots, 2X+9M flares
AR 12673, Sep 2017, 11 hours, 48 snapshots, 2X+1M flares

Moraitis et al. 2024a

flare number	AR	flare class	eruptive (Y/N)	peak time	position	$(E_{\rm div}/E)\times 10^2$
01	11158	M6.6	Y	2011-02-13/17:38UT	S20E04	0.23±0.03
02	11158	X2.2	Y	2011-02-15/01:56UT	S20W10	0.50±0.03
03	11261	M9.3	Y	2011-08-04/03:45UT	N19W36	4.73±0.07
04	11520	X1.4	Y	2012-07-12/16:49UT	S15W01	3.80±0.19
05	11618	M1.7	Y	2012-11-20/12:38UT	N06E20	1.96±0.13
06	11618	M1.6	Y	2012-11-20/19:28UT	N07E15	0.86±0.08
07	11618	M1.4	Y	2012-11-21/06:48UT	N06E10	0.53±0.07
08	11618	M3.5	Y	2012-11-21/15:28UT	N08E14	0.53±0.05
09	11890	M1.0	N	2013-11-05/18:13UT	S12E47	4.70±0.13
10	11890	M2.3	Y	2013-11-07/03:40UT	S14E28	3.97±0.08
11	11890	M2.4	Y	2013-11-07/14:25UT	S13E23	3.60±0.14
12	12192	M4.5	N	2014-10-20/16:37UT	S14E37	1.98±0.08
13	12192	M1.4	N	2014-10-20/19:02UT	S13E43	2.11±0.06
14	12192	M1.7	N	2014-10-20/20:03UT	S13E43	1.88±0.05
15	12192	M1.2	N	2014-10-20/22:55UT	S14E36	2.22±0.03
16	12192	M8.7	N	2014-10-22/01:59UT	S14E19	2.07±0.03
17	12192	M2.7	N	2014-10-22/05:17UT	S14E19	1.79±0.06
18	12192	X1.6	N	2014-10-22/14:28UT	S14E13	2.13±0.05
19	12192	M1.1	N	2014-10-23/09:50UT	S16E03	1.83±0.02
20	12192	M4.0	Y	2014-10-24/07:48UT	S19W06	0.79±0.04
21	12192	X3.1	N	2014-10-24/21:40UT	S16W21	1.15±0.08
22	12673	X2.2	N	2017-09-06/09:10UT	S08W32	4.00±0.50

9 ARs during rising phase of SC24
>40 solar flares
>2000 snapshots
NLFF field extrapolation of ***B***
(Wiegelmann et al. 2012)

Criteria:
- B metrics
- Above M-class flares
- Flares have the highest HMI cadence of 12 min

Statistics:
- 7 ARs in total (2 north – 5 south)
- 11 eruptive – 11 confined flares (9 in AR 12192)
- 5 X – 17 M-class flares

Selection of ROIs

Magnetic polarity inversion line – **MPIL**

Schrijver 2007 method
B_z threshold 150 G
3x3 dilation window
9” FWHM Gaussian

Helicity polarity inversion line – **HPIL**, based on RFLH
10% of max RFLH threshold

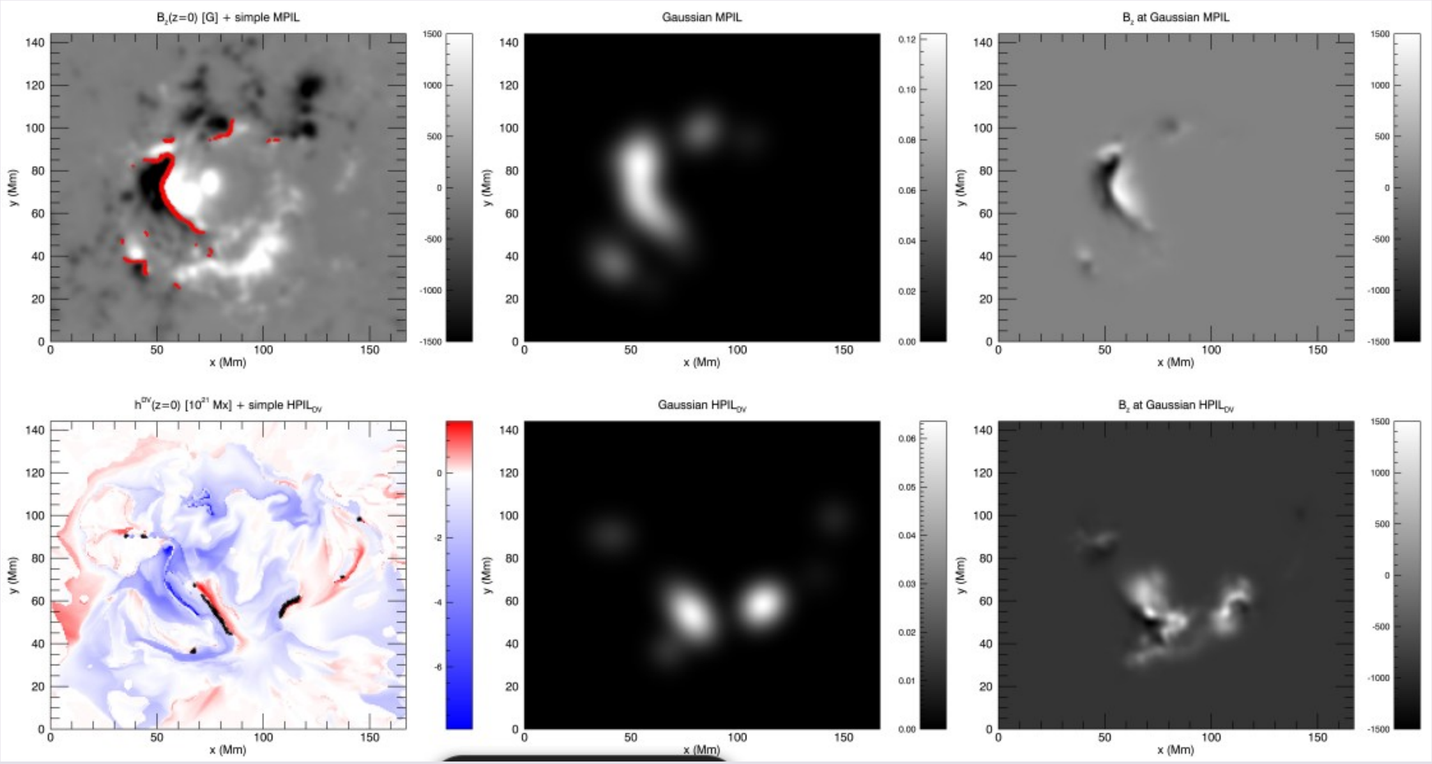

Flare-related helicity profiles

7x relative helicities, of 4 types:

- **Volume method**

$$H_r = \int_V (\mathbf{A} + \mathbf{A}_\mathrm{p}) \cdot (\mathbf{B} - \mathbf{B}_\mathrm{p})\, \mathrm{d}V$$

- **2x RFLH method, DV/BF gauge**

$$H_{\mathrm{r,fl}} = \oint_{\partial V} h_\mathrm{r}\, \mathrm{d}\Phi \simeq \int_{z=0} h_\mathrm{r}\, \mathrm{d}\Phi$$

- **2x MPIL helicities, DV/BF gauge**

$$H_{\mathrm{r,MPIL}} = \int_{z=0} h_\mathrm{r}\, W_{\mathrm{MPIL}}\, \mathrm{d}\Phi$$

- **2x HPIL helicities, DV/BF gauge**

$$H_{\mathrm{r,HPIL}} = \int_{z=0} h_\mathrm{r}\, W_{\mathrm{HPIL}}\, \mathrm{d}\Phi$$

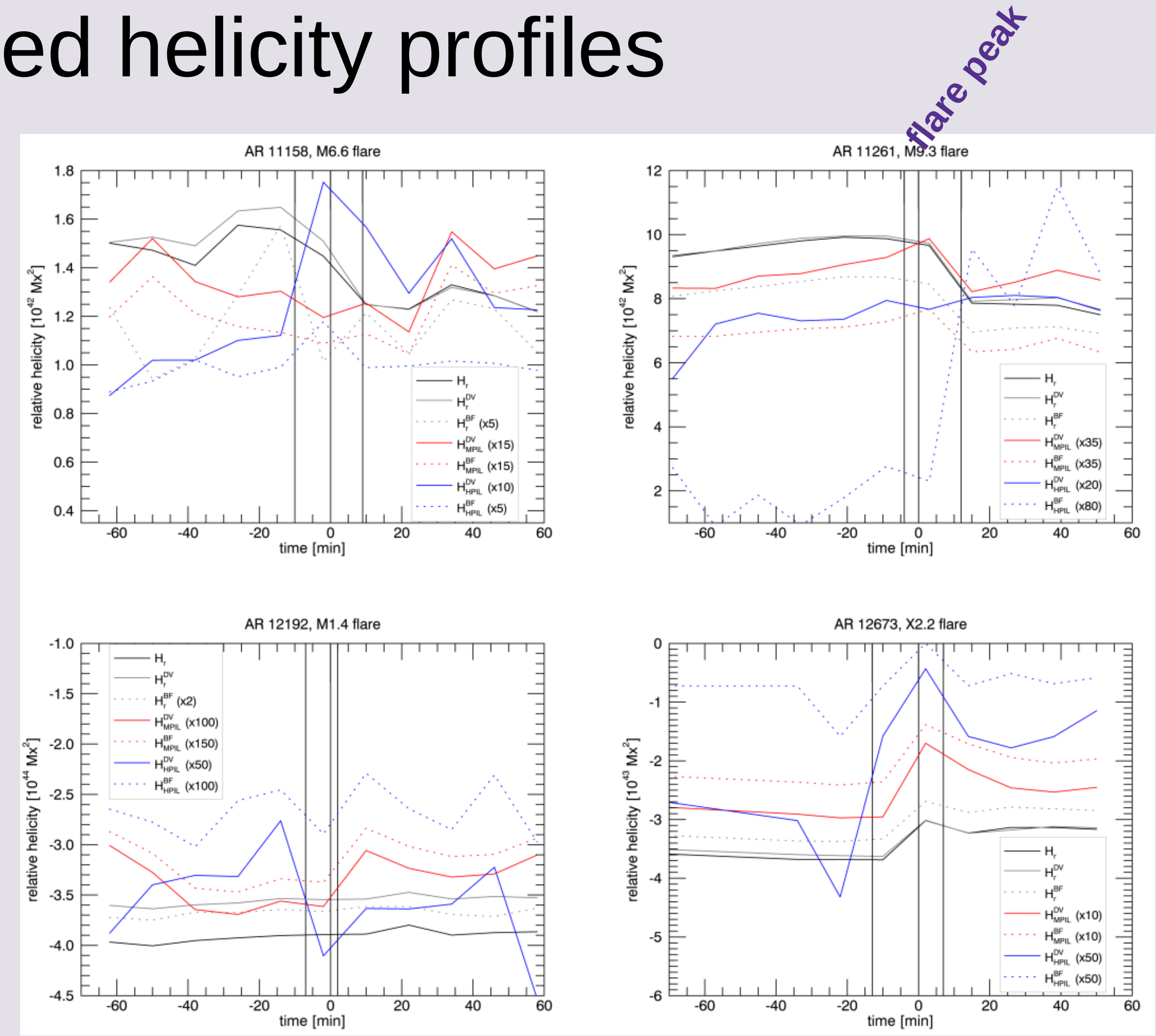

Superposed helicity profiles

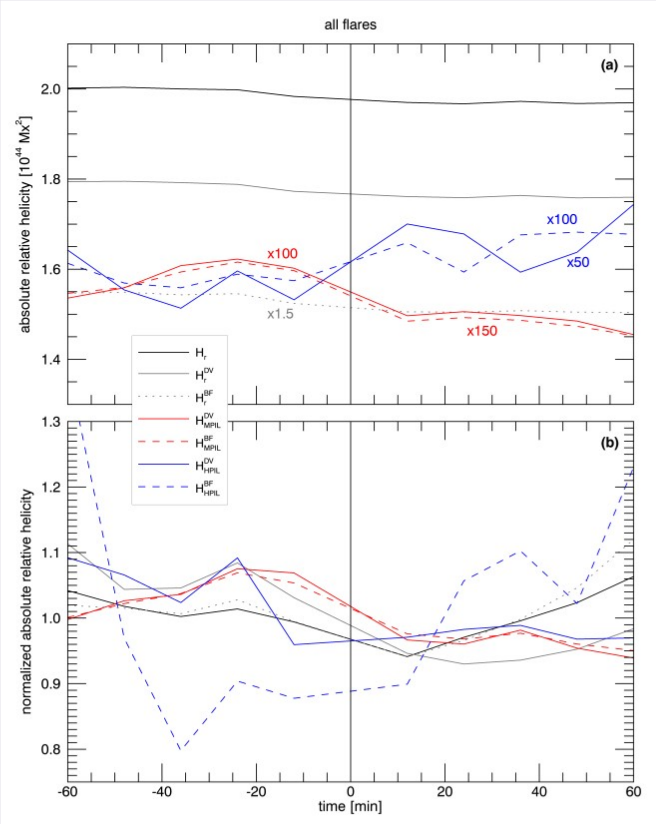

- Superposed epoch analysis of original and normalized profiles
- **Volume** + **fl-helicities** small decrease during flares
- **MPIL helicities** pronounced decrease during flares
- **HPIL helicities** incoherent profiles

f	$\Delta f(\%)$	$\mathrm{D}f(\%)$	f	$\Delta f(\%)$	$\mathrm{D}f(\%)$
H_r	-1.4	-0.7	norm. H_r	-1.5	-5.3
H_r^{DV}	-1.6	-0.7	norm. H_r^{DV}	-10.7	-8.2
H_r^{BF}	-2.4	-1.2	norm. H_r^{BF}	0.13	-5.4
H_{MPIL}^{DV}	-6.2	-6.6	norm. H_{MPIL}^{DV}	-7.7	-9.6
H_{MPIL}^{BF}	-6.6	-7.0	norm. H_{MPIL}^{BF}	-6.8	-7.4
H_{HPIL}^{DV}	6.6	11.0	norm. H_{HPIL}^{DV}	-6.7	1.2
H_{HPIL}^{BF}	4.9	5.4	norm. H_{HPIL}^{BF}	7.6	2.4

Superposed helicity profiles

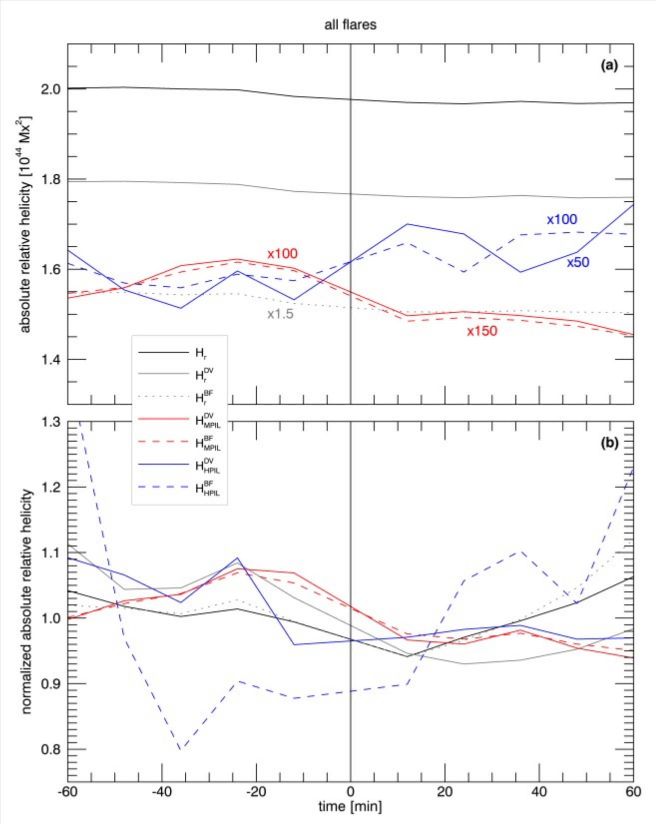

- Superposed epoch analysis of original and normalized profiles
- **Volume** + **fl-helicities** small decrease during flares
- **MPIL helicities** pronounced decrease during flares
- **HPIL helicities** incoherent profiles
- Similar results for original and helicity-based *R*-parameters (Schrijver 2007)

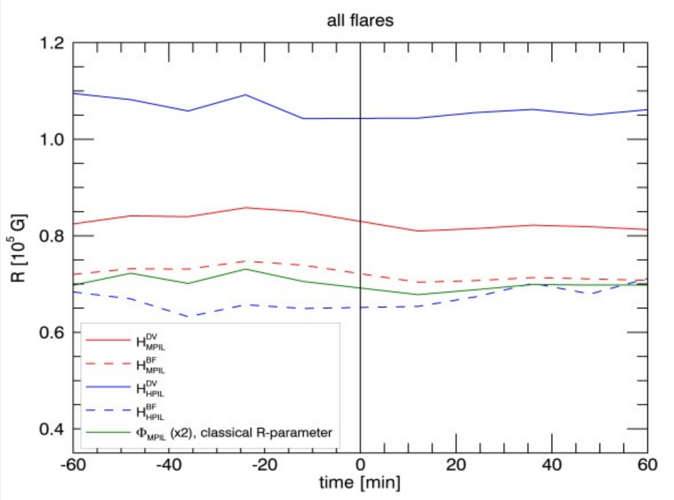

$$R = \int W_{\mathrm{MPIL}}\,\mathrm{d}\Phi/\lambda^2$$

$$R_{\mathrm{H}} = H_{\mathrm{PIL}}^{1/2}/\lambda^2$$

PIL helicities in an MHD simulation

$$H_{\mathrm{r,PIL}} = \int_{z=0} h_{\mathrm{r}}\, W_{\mathrm{PIL}}\, \mathrm{d}\Phi$$

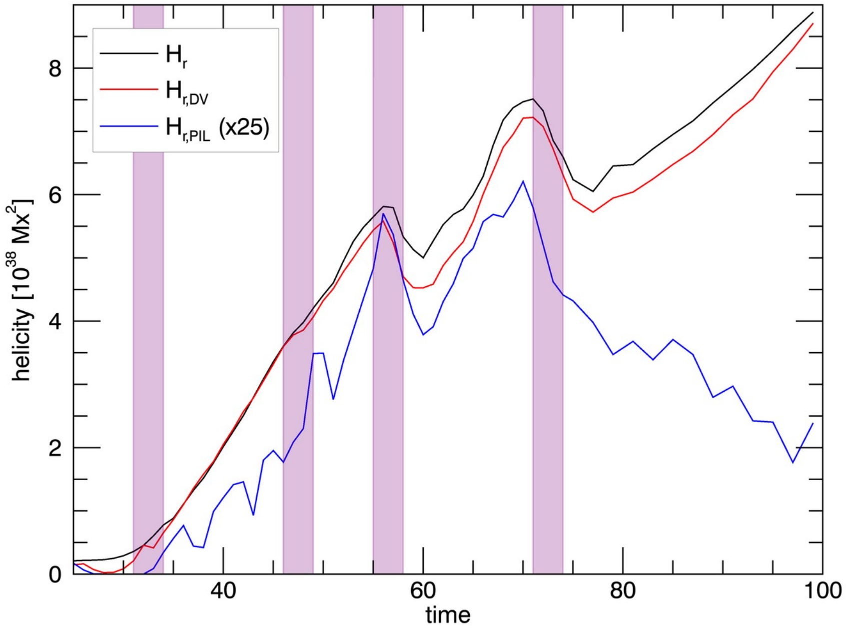

Moraitis et al. 2024b

In an MHD flux emergence simulation of jet production:

- PIL helicity follows H_r until the large blowout jet
- It fluctuates much more and is smaller by ~25
- Too much jiggling during first two jets
- Peaks of $H_{r,PIL}$ near the last two jets more pronounced than H_r
- Difference between $H_{r,PIL}$ and H_r after large blowout jet → increase of the latter due to coronal field
- Confirmation of recent results in a different setup

PIL helicities in an MHD simulation

$$H_{\mathrm{j,PIL}} = \int_{z=0} h_{\mathrm{j}}\, W_{\mathrm{PIL}}\, \mathrm{d}\Phi$$

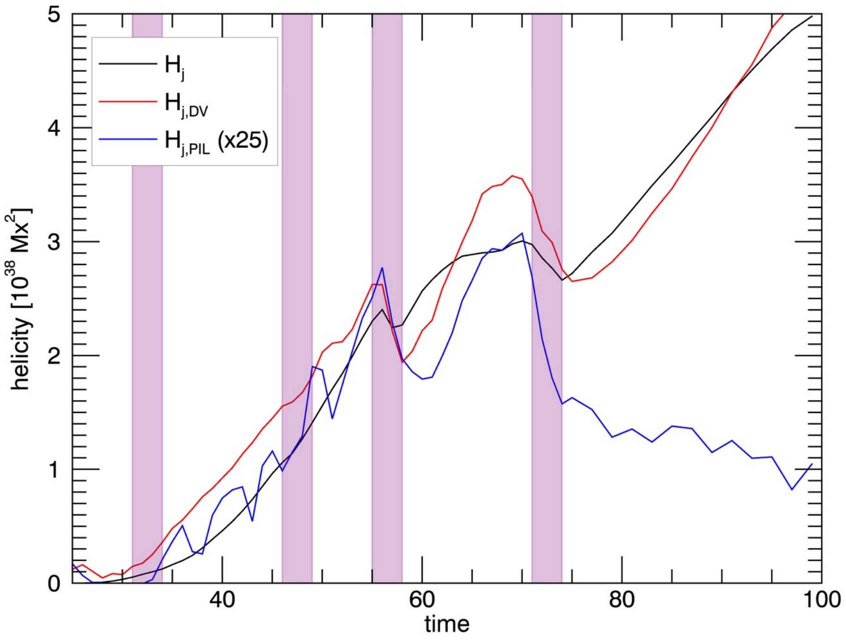

Moraitis et al. 2024b

In an MHD flux emergence simulation of jet production:

- PIL helicity follows H_{r} until the large blowout jet
- It fluctuates much more and is smaller by ~25
- Too much jiggling during first two jets
- Peaks of $H_{\mathrm{r,PIL}}$ near the last two jets more pronounced than H_{r}
- Difference between $H_{\mathrm{r,PIL}}$ and H_{r} after large blowout jet → increase of the latter due to coronal field
- Confirmation of recent results in a different setup
- Computation of $H_{\mathrm{j,PIL}}$ shows similar behaviour

Summary

- (R)FLH a proxy for (relative) helicity density
- RFLH is a useful tool for visualizing important locations for magnetic helicity, but
  - It requires the 3D ***B*** as input
  - Careful with gauge dependence
- RFLH can be used to identify flux ropes in the global magnetic field of the Sun
- In solar ARs, MPIL relative helicity good eruptivity indicator, better than relative helicity, or traditional flux-based *R*-parameter
- Confirmation of importance of MPIL helicity in a jet-producing MHD flux emergence simulation, indications for MPIL current-carrying helicity as well

FLH references

- Antiochos 1987, ApJ, 312, 886
- Berger 1988, A&A, 201, 355
- Yeates & Hornig 2013, Phys. Plasmas, 20, 012102
- Yeates & Hornig 2014, J Phys. Conf. Series, 544, 012002
- Russel et al. 2015, Phys. Plasmas, 22, 032106
- Yeates & Hornig 2016, A&A, 594, A98
- Lowder & Yeates 2017, ApJ, 846, 106
- Aly 2018, Fluid Dyn. Res., 50, 011408
- Yeates & Page 2018, J Plasma Phys., 84, 775840602
- Moraitis et al. 2019, A&A, 624, A51
- Moraitis et al. 2021, A&A, 649, A107
- Yeates et al. 2021, Phys. Plasmas, 28, 082904
- Prior & Yeates 2021, J. Phys. A: Math. Theor., 54, 465701
- Moraitis et al. 2024, A&A, 683, A87
- Yeates & Berger 2024, Geophysical Monograph Series, 283, 1
- Moraitis et al. 2024, A&A, in press